analysis of the space distribution of stars in the solar neighborhood (see §4-2 and §4-3).

The Spectral Type Versus Color, the Color–Color, and Spectral Type Versus Effective-Temperature Relations

The MK spectral type of a star is a concise description of the morphology of its line-spectrum. Inasmuch as both the line and continuous spectrum emitted are determined by the physical structure of a star's atmosphere, we can expect that its continuous energy distribution, and hence colors, will be closely correlated with its MK spectral type. This is indeed found to be the case, and, after allowance for interstellar reddening, one can associate distinctive colors with most types as shown in Table 3-3 for $(B - V)$ and $(U - B)$. [In the table, the data for supergiants represent all subclasses (Ia, Iab, Ib) lumped together unless otherwise indicated.]

The *UBV* color indices clearly show that early-type stars are rich in ultraviolet radiation and that late-type stars are distinctly red. Note that, for the hottest stars, both $(B - V)$ and $(U - B)$ approach limiting values. This is a result of the fact that, at high temperatures ($T \gtrsim 40{,}000$ K), the Planck function in the visible reduces to the Rayleigh–Jeans form $B_\nu(T_R) = (2kT_R\nu^2/hc^2)$, where T_R is a characteristic *radiation temperature* of the radiation field. It follows from equation (2-15) that, in this limit, the color indices will be essentially independent of T_R. The bulk of the radiation emitted by

Table 3-3. The Spectral Type Versus Color Relation

Main sequence (luminosity class V)

Spectral class	$(B - V)$	$(U - B)$	Spectral class	$(B - V)$	$(U - B)$
O5	−0.32	−1.15	B9	−0.06	−0.19
O6	−0.32	−1.14	A0	0.00	0.00
O7	−0.32	−1.14	A5	0.15	0.09
O8	−0.31	−1.13	F0	0.29	0.04
O9	−0.31	−1.12	F5	0.42	−0.01
B0	−0.30	−1.08	G0	0.58	0.05
B1	−0.26	−0.93	G5	0.69	0.20
B2	−0.24	−0.86	K0	0.85	0.47
B3	−0.20	−0.71	K5	1.16	1.09
B5	−0.16	−0.56	M0	1.42	1.25
B7	−0.12	−0.42	M5	1.61	1.22
B8	−0.09	−0.30			

Giants (luminosity class III)

Spectral class	$(B - V)$	$(U - B)$	Spectral class	$(B - V)$	$(U - B)$
O5	−0.32	−1.15	B9	−0.06	−0.19
O6	−0.32	−1.14	A0	0.00	0.00
O7	−0.32	−1.14	A5	0.15	0.10
O8	−0.31	−1.13	F0	0.27	0.10
O9	−0.31	−1.12	F5	0.45	0.07
B0	−0.30	−1.09	G0	0.65	0.30
B1	−0.26	−0.95	G5	0.84	0.52
B2	−0.24	−0.88	K0	1.03	0.87
B3	−0.20	−0.72	K5	1.45	1.65
B5	−0.16	−0.56	M0	1.57	1.8
B7	−0.12	−0.42	M5	1.80	2.1
B8	−0.09	−0.30			

Table 3-3. (*continued*)

Supergiants (luminosity class I)

Spectral class	$(B - V)$	$(U - B)_{Ib}$	$(U - B)_{I}$	$(U - B)_{Ia}$
O5	−0.32		−1.16	
O6	−0.32		−1.15	
O7	−0.31		−1.14	
O8	−0.29		−1.13	
O9	−0.28		−1.12	
B0	−0.24	−1.05		−1.07
B1	−0.19	−0.96		−1.00
B2	−0.17	−0.91		−0.96
B3	−0.13	−0.82		−0.87
B5	−0.09	−0.72		−0.78
B7	−0.05	−0.62		−0.68
B8	−0.02	−0.53		−0.60
B9	0.00	−0.48		−0.56
A0	0.01		−0.35	
A5	0.07		...	
F0	0.21		0.22	
F5	0.40		0.30	
G0	0.70		0.60	
G5	1.07		0.83	
K0	1.37		1.35	
K5	1.65		1.7	
M0	1.9		1.7	
M5	2.1		1.8	

SOURCES: Adapted from (**A3**, 206), (**G3**, 79), (**S24**, 214)

Table 3-4. Infrared Colors of Main-Sequence Stars

Spectral class	Color index					
	$(V-R)$	$(V-I)$	$(V-J)$	$(V-K)$	$(V-L)$	$(V-N)$
A0	0.00	0.00	0.00	0.00	0.00	0.00
F0	0.30	0.47	0.55	0.74	0.8	0.8
G0	0.52	0.93	1.02	1.35	1.5	1.4
K0	0.74	1.4	1.5	2.0	2.5	
M0	1.1	2.2	2.3	3.5	4.3	
M5	...	2.8				

SOURCE: (**A3**, 208), by permission

late-type stars emanates in the infrared as is shown clearly in Table 3-4. Similarly, colors constructed from far-ultraviolet magnitudes (observed from space) and V show that the peak energy emission by early-type stars moves to progressively shorter wavelengths as the temperature of the stellar atmosphere rises.

The data in Table 3-3 can be used to construct *color-color* (or *two-color*) *diagrams*, such as those shown in Figure 3-7. As can be seen, it is possible to distinguish stars of different spectral and luminosity classes from one another, assuming that adequate allowance can be made for interstellar reddening. Similar diagrams using other photometric indices can sometimes be used to carry out a two-dimensional photometric "spectral classification"

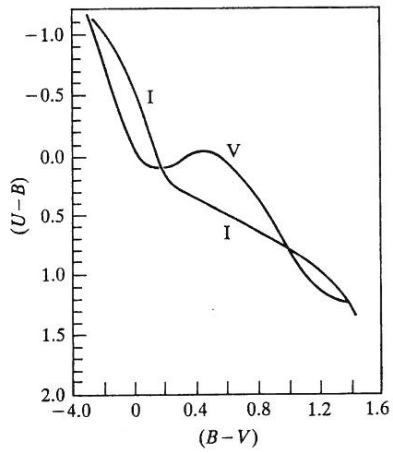

Figure 3-7. Two-color diagram for main-sequence stars (luminosity class V) and supergiants (luminosity class I).

Table 3-5. The Effective-Temperature and Bolometric-Correction Scales

Spectral class	Luminosity class V		Luminosity class III		Luminosity class I	
	T_{eff}	*B.C.*	T_{eff}	*B.C.*	T_{eff}	*B.C.*
O5	47,000	−4.0				
O7	38,000	−3.5				
O9	34,000	−3.2			30,000	−2.9
B0	30,500	−3.00			25,500	−2.6
B2	23,000	−2.30				
B3	18,500	−1.85				
B5	15,000	−1.40			13,500	−0.9
B7	13,000	−0.90				
B8	12,000	−0.70				
A0	9,500	−0.20				
A5	8,300	−0.10				
F0	7,300	−0.08			6,400	−0.2
F5	6,600	−0.01				
G0	5,900	−0.05	5,400	−0.1	5,400	−0.3
G5	5,600	−0.10	4,800	−0.3	4,700	−0.6
K0	5,100	−0.2	4,400	−0.5	4,000	−1.0
K5	4,200	−0.6	3,600	−1.1	3,400	−1.6
M0	3,700	−1.2	3,300	−1.5	2,800	−2.5
M5	3,000	−2.5	2,700:	−3:		
M8	2,500	−4:				

SOURCES: Adapted from (**A3**, 206), (**C13**), (**J2**)

within limited regions of the H-R diagram. This is valuable because we can then classify very faint stars.

As was discussed in §3-4, the spectrum of a star is essentially determined by its effective temperature and surface gravity. Furthermore, because a stellar spectrum can be characterized by giving its MK spectral type, it follows that, to each MK spectral type, there should correspond definite values of T_{eff}, *B.C.*, and the surface gravity g. In §3-4, we described various methods for determining T_{eff}; Table 3-5 assembles representative results of this work. The most reliable values given are for main-sequence $B-K$ stars. The accuracy of the estimates deteriorates for O and M stars and for giants and supergiants. Table 3-5 shows that MK spectral classes correlate closely with T_{eff}. The MK luminosity classes are primarily sensitive to the surface gravity g. The relationships $L \propto R^2 T_{\text{eff}}^4$ and $g \propto \mathcal{M}/R^2$ imply $L \propto (\mathcal{M}/g)$ at fixed spectral type (fixed T_{eff}). Figure (3-8) shows how the luminosity of

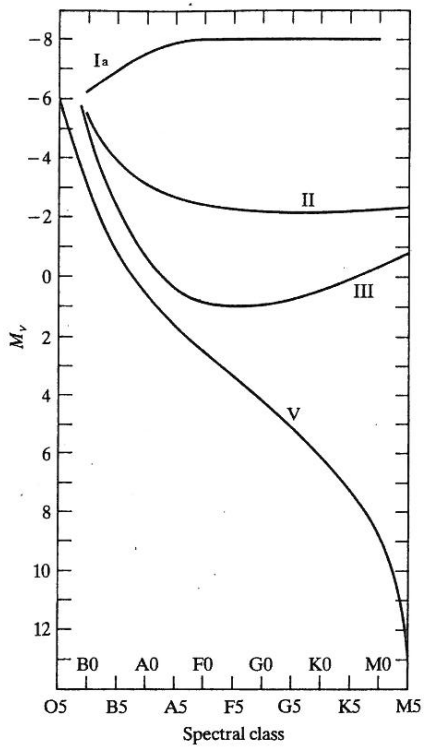

Figure 3-8. Absolute visual magnitude as a function of MK spectral type. Individual curves are labeled with luminosity classes.

a star depends on its MK spectral type. High-luminosity stars tend to have large masses and low gravities.

The Mass-Luminosity and Mass-Radius Relations

Naively, one would expect massive stars to be very luminous and stars with small masses to be faint. Broadly speaking, it is true that faint stars have small masses, but it turns out that luminous stars are not necessarily massive. As we shall see, the luminosity of a star tends to increase as it evolves, and this increase is very pronounced for low-mass stars. Thus, toward the end of its life, even quite a low-mass star can become a luminous giant. If one confines one's attention to main-sequence stars, however (and, in any given cluster, most stars will at any one time be on the main sequence), one finds

Table 3-6. Physical Properties of Main-Sequence Stars

$\log(\mathcal{M}/\mathcal{M}_\odot)$	Spectral class	$\log(L/L_\odot)$	M_{bol}	M_V	$\log(R/R_\odot)$
−1.0	M6	−2.9	12.1	15.5	−0.9
−0.8	M5	−2.5	10.9	13.9	−0.7
−0.6	M4	−2.0	9.7	12.2	−0.5
−0.4	M2	−1.5	8.4	10.2	−0.3
−0.2	K5	−0.8	6.6	7.5	−0.14
0.0	G2	0.0	4.7	4.8	0.00
0.2	F0	0.8	2.7	2.7	0.10
0.4	A2	1.6	0.7	1.1	0.32
0.6	B8	2.3	−1.1	−0.2	0.49
0.8	B5	3.0	−2.9	−1.1	0.58
1.0	B3	3.7	−4.6	−2.2	0.72
1.2	B0	4.4	−6.3	−3.4	0.86
1.4	O8	4.9	−7.6	−4.6	1.00
1.6	O5	5.4	−8.9	−5.6	1.15
1.8	O4	6.0	−10.2	−6.3	1.3

SOURCE: Adapted from (**A3**, 209), by permission

both empirically and theoretically that a *mass-luminosity relation* holds; $L \propto \mathcal{M}^{3.2}$, approximately. For main-sequence stars, there is also a *mass-radius relation*; $R \approx R_\odot(\mathcal{M}/\mathcal{M}_\odot)^{0.7}$. These results, which are summarized in Table 3-6, can be explained satisfactorily by the theory of stellar structure.

A very important consequence of the main-sequence mass-luminosity relation and the tendency of the luminosity of a star to increase as it evolves is that luminous stars must have lifetimes much shorter than the Sun's. The amount of fuel available for thermonuclear burning is approximately proportional to a star's mass, and the rate at which it is consumed is proportional to its luminosity. Hence the lifetime τ of a star is proportional to $\mathcal{M}/\bar{L}$, where $\bar{L}$ is the mean luminosity of a star averaged over its lifetime. Because stars leave the main sequence only when they are running short of fuel and then rapidly squander their slender remaining reserves, a star's mean luminosity $\bar{L}$ does not differ significantly from its main-sequence luminosity L_{ms}. Therefore, from the main-sequence mass-luminosity relation, we can estimate for the lifetime, $\tau \propto \mathcal{M}/L_{ms} \propto \mathcal{M}^{-2.2}$. It is thus clear that massive stars have short lifetimes. In fact, the theory of stellar structure predicts [see equation (3-44)] that an O star cannot live longer than about a million years.

It was essentially this quite simple calculation that led L. Spitzer to conclude (**S20**) in 1948 that star formation must be a continuous, ongoing process. The mere existence of very luminous stars indicates that not all star formation can have occurred in the distant past. To determine how the

Table 3-7. Correlation of Stellar Radius and Luminosity with MK Spectral Type

Spectral class	$\log(R/R_\odot)$			$\log(L/L_\odot)$		
	V	III	I	V	III	I
O5	1.25			5.7		
B0	0.87	1.2	1.3	4.3		5.4
B5	0.58	1.0	1.5	2.9		4.8
A0	0.40	0.8	1.6	1.9		4.3
A5	0.24		1.7	1.3		4.0
F0	0.13		1.8	0.8		3.9
F5	0.08	0.6	1.9	0.4		3.8
G0	0.02	0.8	2.0	0.1	1.5	3.8
G5	−.03	1.0	2.1	−0.1	1.7	3.8
K0	−.07	1.2	2.3	−0.4	1.9	3.9
K5	−.13	1.4	2.6	−0.8	2.3	4.2
M0	−.20		2.7	−1.2	2.6	4.5
M5	−.5			−2.1	3.0	

SOURCE: Adapted from (**A3**, 209), by permission

rate of star formation changes in time is an important task of the theory of *galactic evolution.* Conversely, any such theory will be constrained in significant ways by the numbers of stars with various masses observed to exist at present, essentially because there *is* a characteristic lifetime for each mass, which implies that a study of stars of decreasing mass gives a glimpse of our Galaxy at increasing mean stellar age and hence at increasing look-back times.

Each MK spectral type is associated with characteristic values of L and R. Table 3-7 gives typical values for these quantities, expressed in solar units. The great range of R values quoted in Table 3-7 for M stars follows from the huge range of luminosities displayed by these stars, which all have similar effective temperatures. Actually, the range in the radii of stars is even greater than this table would suggest. Some of these stars are 1000 solar radii in diameter, whereas a typical white dwarf has a radius of about $10^{-2}R_\odot$, comparable to that of the Earth. The mean densities of stars vary over a correspondingly gigantic range, from less than 10^{-6} of the solar mean density for the typical red giant to nearly 10^6 of solar for a white dwarf. The latter are, in fact, so dense that they are sustained against gravitational collapse by the zero-point energies of their electrons, just as an atom is sustained against electrostatic collapse by the residual motion of its electrons. One says that the material of white dwarfs is *degenerate.* During the life of a star, its radius, and hence its mean density, will change considerably. Its

mass may also change as a result of mass loss or mass exchange, but this change is probably a less important phenomenon than the change in radius. In any case, we do not know how to model mass loss theoretically.

3-6. SYSTEMATICS OF STELLAR PROPERTIES: SPHEROIDAL-COMPONENT STARS

In addition to the metal-rich stars in the disk and spiral arms, our Galaxy contains a second major group of stars in its *spheroidal component.* These stars are represented in the solar neighborhood by the metal-poor *subdwarfs* and at larger distances by the stars in *globular clusters* and the *galactic bulge.* The physical properties of spheroidal-component stars are quite different from those of disk stars, and this fact is clearly manifested in their H-R and CM diagrams. As was mentioned in Chapter 1, these stars are all old and have a very different history from the disk stars. In all probability, they were formed before the disk itself existed.

The Subdwarfs

Among the F, G, and K stars observed in the neighborhood of the Sun are a few that fall distinctly below the main sequence in a CM diagram. Because they appear somewhat underluminous (in M_V) for their $(B - V)$ color, these stars are called subdwarfs. Compared to common field stars, the subdwarfs also have an *ultraviolet excess*; that is, they have brighter $(U - B)$ colors than normal stars having the same $(B - V)$.

When the subdwarfs are examined spectroscopically, it is found that their spectral lines are abnormally weak, and quantitative spectroscopic analyses show them to be extremely metal poor relative to the Sun, with abundances down by a factor of 10^{-2} or more. As soon as it was known that the subdwarfs are weak lined, it was recognized that this implied that they should appear to be too blue relative to stars having normal line strengths but otherwise identical properties (L and T_{eff}). In turn, it was realized that they might appear to be subdwarfs in a CM diagram, not because they are really underluminous but rather because they are anomalously blue and therefore displaced to the left of the normal main sequence.

Thus, to compare stars with markedly different compositions, we must be able to account for the effects of different metal abundances on photometric indices and to determine the position of a star of arbitrary metal abundance relative to some fiducial sequence (the Hyades is invariably used as the standard) in both CM diagrams and the theoretical H-R diagram. Furthermore, we must develop methods that allow photometric indices to be used directly to infer information about the metal content of stars. To accomplish these goals, we must evaluate the photometric effects of line-blanketing in

stars with differing metal abundances. In the following discussion, we shall focus mainly on blanketing corrections in the *UBV* system because this system reaches the faintest stars and has been widely used, for example, in studies of globular clusters. Similar considerations apply to other systems as well.

Line-Blanketing The mere presence of dark spectral lines in any photometric band obviously reduces the energy emitted in that band. This direct effect of *line-blocking* is described by the *blocking coefficient*

$$\varepsilon_\lambda \equiv 1 - \left[\frac{\int_{\lambda-\Delta\lambda}^{\lambda+\Delta\lambda} F_\lambda \, d\lambda}{\int_{\lambda-\Delta\lambda}^{\lambda+\Delta\lambda} F_\lambda^c \, d\lambda} \right] \tag{3-36}$$

where F_λ denotes the observed flux at wavelength λ, F_λ^c is the continuum flux near λ, and $\Delta\lambda$ is a prechosen wavelength interval (typically 25 Å to 50 Å). Blocking coefficients have been measured by direct planimetry of tracings of high-dispersion spectra for a variety of stars (**M14**), (**W7**); some typical results are shown in Figure 3-9. The basic points to be noticed in the figure are that (1) the blocking coefficient increases rapidly from the visual toward the blue and ultraviolet (indeed, so strongly that, in the ultraviolet, it is difficult to find unblocked windows within which to set the continuum level) and (2) the later the spectral type of a star, the larger is the amount of line-blocking. Notice particularly in Figure 3-9*b* how much weaker the blocking is in the subdwarf HD 19445 than it is in the Sun. Trustworthy blocking coefficients for very late-type stars are almost impossible to determine empirically, because the lines simply swamp the continuum and there is no way to set the continuum-flux level reliably in much of the visible spectrum.

From the variation of ε_λ with wavelength, it is clear that, if we start with a star having zero metal abundance and therefore no spectrum lines (other than hydrogen lines) and gradually increase the metal abundance up to the Hyades value, the star should become fainter in $(B - V)$ and fainter yet in $(U - B)$. But these line-blocking effects produce only part of the total blanketing effect. An additional effect of increasing the metal abundance while holding a star's effective temperature constant is *backwarming* of the atmosphere. If we demand that the same total energy flux (which is fixed by thermonuclear processes in the star's interior) must ultimately escape from the star (that is, that T_{eff} remains constant), then the energy blocked in the lines must be redistributed in wavelength and escape from continuum windows between the lines. This redistribution raises the continuum level above the value it would have had in the absence of lines, and it simulates the effect of a higher effective temperature of the star. The net photometric changes produced by adding lines are determined by a competition between these two effects, blocking tending to increase each observed magnitude and

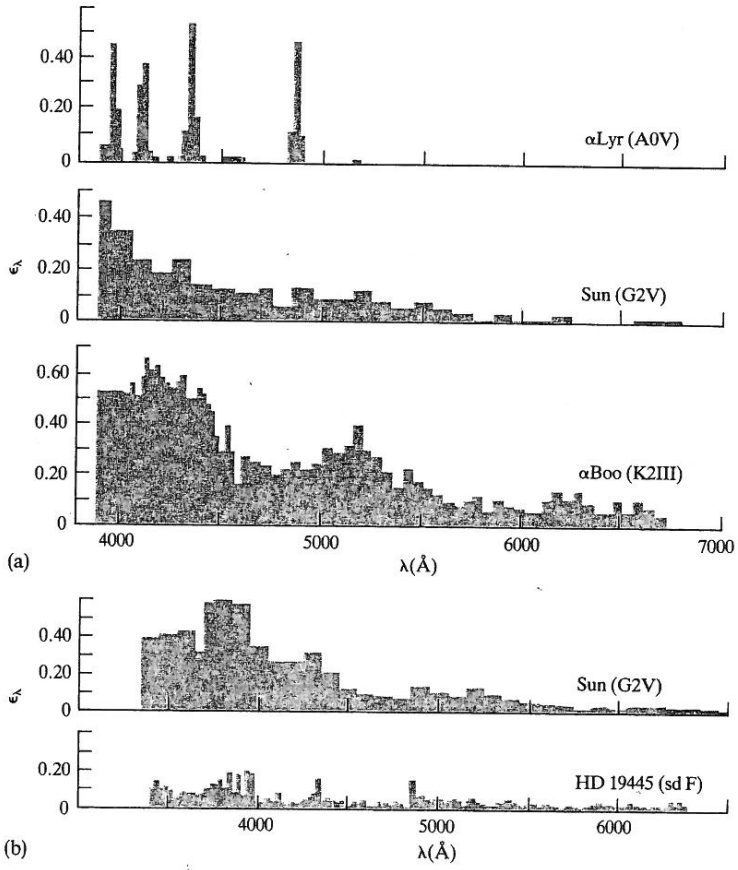

Figure 3-9. Observed line-blocking coefficients for (a) an early-type dwarf (α Lyr), the Sun, and a late-type giant (α Boo); and (b) the Sun and an extreme subdwarf, HD 19445. *Ordinate*: ε_λ as defined in equation (3-36); *abscissa*: wavelength in Ångstroms. [Adapted from (**M14**) and (**W7**) by permission. The latter is © 1962 by the University of Chicago.]

backwarming tending to decrease it. In practice, blocking dominates over backwarming in the *U* band, exceeds it slightly in the *B* band, and is less important in the *V* band; in the end, adding lines increases $(U - B)$ and $(B - V)$ and decreases *V*.

The final result in the two-color diagram is that the star moves along a *blanketing vector*, such as that shown in Figure 3-10. We see in the figure

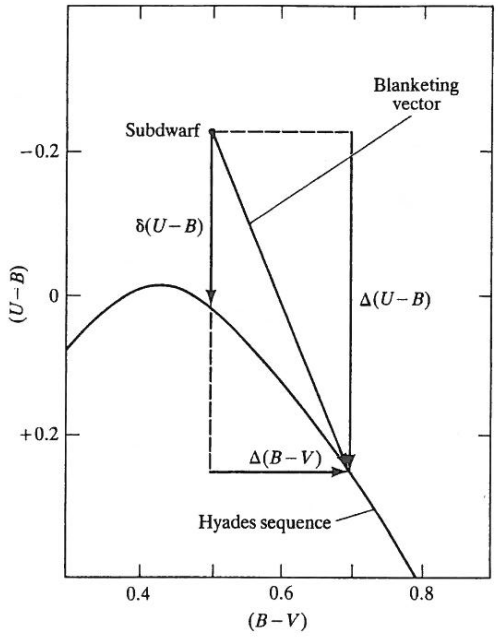

Figure 3-10. Blanketing vector in two-color diagram for a metal-deficient subdwarf. The subdwarf has an ultraviolet excess $\delta(U - B)$ compared to a Hyades star (which has near-solar metal abundance) of the same $(B - V)$. A Hyades star *of the same effective temperature* has colors that differ by amounts $\Delta(B - V)$ and $\Delta(U - B)$ from those of the subdwarf. The effect of adding metal lines to the subdwarf's atmosphere while holding T_{eff} constant is to move the observed colors along the blanketing vector as defined in (**S3**) and (**W7**).

that a metal-poor star that has an *ultraviolet excess* $\delta(U - B)$ relative to Hyades stars having the same $(B - V)$ will differ from Hyades stars of the same effective temperature by amounts $\Delta(B - V)$ and $\Delta(U - B)$ in $(B - V)$ and $(U - B)$, respectively. If we can determine the slope of blanketing vectors as a function of $(B - V)_{\text{Hyades}}$, then we can clearly determine the *blanketing corrections* $\Delta(B - V)$ and $\Delta(U - B)$ for any star of known $\delta(U - B)$ and $(B - V)$. If, in addition, we can calculate ΔV, we are then in a position to correct the observed colors and brightnesses of stars for differential blanketing effects and thus map cluster CM diagrams onto one another, reduced to a common abundance.

Empirical blanketing vectors have been derived by Wildey et al. (**W7**). Blocking effects were calculated directly as

$$\Delta m_{\text{bk}} = 2.5 \log \left[\frac{\int_{\lambda_1}^{\lambda_2} F_\lambda S_\lambda \, d\lambda}{\int_{\lambda_1}^{\lambda_2} F_\lambda (1 - \varepsilon_\lambda) S_\lambda \, d\lambda} \right] \tag{3-37}$$

where S_λ is the photometer response on the interval (λ_1, λ_2). To compute the backwarming effect, the *integrated blocking coefficient*

$$\eta \equiv \frac{\int_0^\infty \varepsilon_\lambda F_\lambda \, d\lambda}{\int_0^\infty F_\lambda \, d\lambda} \tag{3-38}$$

is used to evaluate T_1, the (larger) effective temperature of an atmosphere that has the same continuum level as does the backwarmed line-blanketed atmosphere, whose actual effective temperature is T_2, from the relation

$$(1 - \eta)\sigma T_1^4 = \sigma T_2^4 = \int_0^\infty F_\lambda \, d\lambda \tag{3-39}$$

The magnitude change produced by the backwarming effect is then

$$\Delta m_{\text{bw}} = 2.5 \log \left[\frac{\int_{\lambda_1}^{\lambda_2} F_\lambda(T_1) S_\lambda \, d\lambda}{\int_{\lambda_1}^{\lambda_2} F_\lambda(T_2) S_\lambda \, d\lambda} \right] \tag{3-40}$$

To actually evaluate this expression, one must use fluxes from model atmospheres at the appropriate effective temperatures.

Applying equations (3-37) and (3-40), one can compute the net changes in ΔU, ΔB, and ΔV produced by the combined effects of blocking and backwarming. These results can then be used to construct tables (**W7**) or graphs (**B7**, 365) giving $\Delta(B - V) = f[\delta(U - B), (B - V)_{\text{obs}}]$, and similar relations for $\Delta(U - B)$ and ΔV. By custom, $\delta(U - B)$ is taken as increasingly positive for more metal-deficient stars; to map such stars onto the Hyades sequence, one will have $\Delta(U - B) > 0$, $\Delta(B - V) > 0$, and $\Delta V < 0$. For example, the Hyades are slightly metal rich compared to the Sun, and one finds $\Delta(U - B)_\odot \approx 0.07$, $\Delta(B - V)_\odot \approx 0.055$, $\Delta(U - B)_\odot \approx 0.13$, and $\Delta V_\odot \approx -0.026$.

Thanks to recent advances in model-atmosphere calculations, blanketing vectors can now also be determined theoretically [see (**B5**), (**G8**), (**N3**), (**P6**, 271), and (**P6**, 319)]. An example of such work is shown in Figure 3-11. Similar calculations can also be made for other photometric systems, such as the Strömgren *uvby* system. It is worth noting that theoretical model atmosphere analyses of subdwarf spectra are actually easier than for ordinary stars because the subdwarfs' line spectrum is so weak, and accurate effective

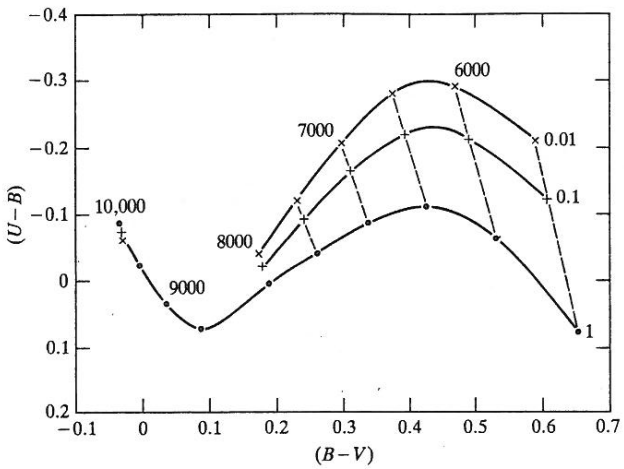

Figure 3-11. Theoretical $(U - B)$ and $(B - V)$ colors for model atmospheres having $\log g = 4$ and effective temperatures between 5500 K and 10,000 K. *Solid dots*: normal solar metal abundance. *Plus signs*: 0.1 times solar metal-abundance. x's: 0.01 times solar metal abundance. Dashed lines show the resulting theoretical blanketing vectors. [From **(P6**, 271).]

temperatures can be obtained for these stars by fitting their observed absolute energy distributions to theoretical fluxes, as was first done by Melbourne **(M11)**. Certain photometric indices, for example, $(G-I)$ in the six-color system, are almost unaffected by blanketing effects in F–K stars because the blocking and backwarming effects almost exactly cancel **(C12)**, **(D2)**. For nearly solar-type stars, such indices can thus be used to make fairly reliable estimates of T_{eff} for stars of all metallicities.

Photometric Metal-Content Indicators By combining photometric data for subdwarfs with spectroscopically determined metal abundances, one can calibrate a photometric index, say, the ultraviolet excess $\delta(U - B)$, in terms of a star's metal abundance. This index can then be used to estimate metal abundances in other stars, a procedure that is highly advantageous because (1) many stars of interest that are too faint for high-dispersion spectroscopy (the practical limit is $m \approx 12$) can be measured with UBV photometry (practical limit $m \approx 20$), and (2) several days of laborious measurement and analysis are required to produce a spectroscopic abundance estimate even when spectra are available, whereas a photometric determination requires only a small fraction of this effort.

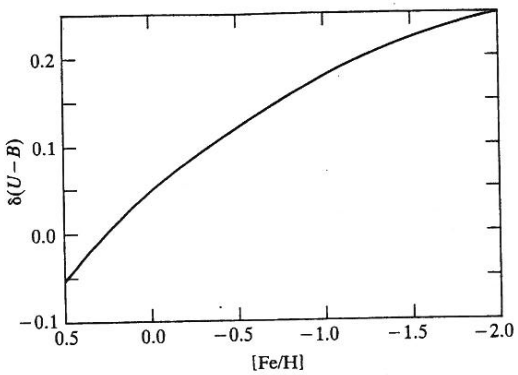

Figure 3-12. Correlation of the ultraviolet excess $\delta(U - B)$, measured with respect to the Hyades sequence, with logarithmic metal abundance [Fe/H] relative to the Sun.

Metal abundances are usually expressed in terms of the stellar iron-to-hydrogen ratio compared to that of the Sun via the parameter

$$[\text{Fe/H}] \equiv \log[n(\text{Fe})/n(\text{H})]_* - \log[n(\text{Fe})/n(\text{H})]_\odot \qquad (3\text{-}41)$$

The correlation of $\delta(U - B)$ with [Fe/H] has been established by several investigations [see **(B9)**, **(E3)**, **(H10)**, **(P1)**, **(P9)**, **(W1)**, **(W2)**], and a representative curve is shown in Figure 3-12; it should be recalled that $\delta(U - B)$ is measured with respect to the Hyades, which has $[\text{Fe/H}]_{\text{Hyades}} \approx +0.025$. For modest values of $\delta(U - B)$, the relation

$$[\text{Fe/H}] - [\text{Fe/H}]_{\text{Hyades}} \approx -5\delta(U - B) \qquad (3\text{-}42)$$

can be used for $\delta(U - B)$ both greater than or less than zero (the latter applying to metal-rich stars).

Similarly, in the Strömgren system (see §2-6), if Δm_1 is the difference between the m_1 index of a star and that of a Hyades star of the same $(b - y)$, then one finds **(G8)**, **(N3)**

$$[\text{Fe/H}] - [\text{Fe/H}]_{\text{Hyades}} \approx -14\Delta m_1, \qquad [0.2 \le (b - y) \le 0.3] \quad (3\text{-}43a)$$

and

$$[\text{Fe/H}] - [\text{Fe/H}]_{\text{Hyades}} \approx -12.5\Delta m_1, \qquad [0.3 < (b - y) < 0.4] \quad (3\text{-}43b)$$

Calibrations also exist for other photometric systems [see, for example, **(P6)**].